Airframe Noise Reduction for a Wing-flap Configuration using DBD Plasma Actuators

Sahan Wasala[*], Shia-Hui Peng[†], Hua-Dong Yao[‡] and Lars Davidson[§]

Chalmers University of Technology , Gothenburg 41296, Sweden

Airframe is considered to be one of the primary noise sources during aircraft take off and landing maneuvers, causing disturbance to the people living vicinity to airports. With the increasing demand for air transportation, there is need to innovate new technologies to reduce airframe noise. High lift device noise, in particular the wing-flap noise, gives a considerable contribution to the total airframe noise levels. This paper investigates the noise from a simplified wing-flap configuration and possibility of reducing the noise with the use of a Dielectric Barrier Discharge (DBD) plasma actuator. A compressible SST k-ω based Improved Delayed Detached Eddy Simulation (IDDES) has been used to simulate the unsteady flow field. The Ffowcs-Williams & Hawkings (FW-H) acoustic analogy has been used to predict the far field noise. The effects of plasma has been modeled as volumetric body force source, based on the Suzen and Huang model. Results indicate a noise reduction of about 2.5 dB at frequencies below 1 kHz, as electric potential increases to 20 kV.

Nomenclature

C_p	=	pressure coefficient
C_{Prms}	=	coefficient of pressure fluctuations
C_{flap}	=	chord of the flap [m]
C_{wing}	=	chord of the wing [m]
Δt	=	time step [s]
$\vec{E}$	=	electric field [N/C]
$\vec{f_b}$	=	body force vector due to plasma [N/m^3]
ρ_c	=	charge density [C/m^3]

I. Introduction

Aircraft noise is a major concern for communities around airports, in particular with the growing demand in the civil aviation industry [1]. This emphasizes the need of identifying the aircraft noise sources and innovate new technologies to mitigate noise levels. Aircraft have two main noise sources; engine and airframe. Total engine noise is a combination of the noise from its internal components such as fan, compressor, turbine and jet. This has been considerably reduced with the increase of the by-pass-ratio of modern turbo fan engines [2]. Airframe noise, on the other hand, originate from the landing gear and high lift devices (e.g. flaps, slats). Here, the high lift devices involves in noise generation mechanisms because of unsteady aerodynamic phenomena such as vortex recirculation, free shear layer vortex flow reattachment, and tonal noise due to edge scattering. Slat noise is mainly tonal. Flap noise has a broadband nature and is louder at high angles of attack [3]. In addition to this, tonal noise can be generated on flaps because of the

vortex formation at the side edges [4]. Previous attempts of understanding and reducing flap noise was conducted in EU projects VALIANT, ATAAC, RAIN, TIMPANN, SADE, OPENAIR [5]. The VALIANT and ATAAC projects focused on understanding the airframe noise generation mechanisms by means of experimental and numerical tools. Furthermore, the VALIANT project addressed the aircraft noise by focusing on high lift devices, in particular using the wing-flap configuration. Salas et al.[6] simulated the full wing-flap configuration, that was previously used in the VALIANT project, using LES. They observed more laminar behavior on the high lift device with tones that could be due to the feedback loop between the trailing edge noise and transitional boundary layer of the flap. RAIN, TIMPANN, SADE, OPENAIR projects focused on reducing the noise levels from high lift devices, where noise reduction methods such as use of porous materials, brushes, micro tabs etc have shown to be very effective [7].

European Union vision 2020 that targets reducing aircraft noise levels by 10 dB, compared to the year 2000, require more innovative technologies. Active flow control using Dielectric Barrier Discharge (DBD) plasma and/or other air blowing/suction methods may help to achieve those goals. DBD plasma actuators have rarely been proposed for noise control, however they have been widely studied for aerofoil flow control [8], [9], [10]. Aerodynamic flow properties, such as vortex generation and interaction with the aerofoil trailing edges, are the cause for aeroacoustic noise sources. Therefore as a consequence, noise generation could be mitigated using DBD plasma actuators by manipulating flow properties, usually, alleviating or even diminishing flow separation and/or the intensity of vortex motions [11].

Accurate numerical modeling of a plasma actuators is complex. Therefore more phenomenological electrostatic models and linearized force models have been developed to mimic the effects of DBD plasma actuation. Models developed by Suzen & Huang (S-H) [12] and Orlov & Corke (O-C) [13] are examples of electro static models. In S-H model, the electric field due to the electrodes and charged particles are calculated separately. The first part is solved using the Poisson equation. The second part is solved based on a simple model of the charge density at the wall, where it is assumed to have a Gaussian distribution. This distribution function is voltage independent and plasma is time independent therefore this could lead to erroneous body force distribution. However the model is simple to use and have been widely tested. Orlov & Corke developed a relatively detailed plasma model where actuators are modeled as a network of air capacitors, dielectric capacitors, plasma resistive elements and diodes in an electric circuit. Unlike the S-H model O-C model is time dependent. However, the model coefficients, which are frequency and voltage dependent, are empirically determined, therefore valid only for the given frequency and voltage.

This paper focuses on aeroacoustic noise reduction using DBD plasma actuators on a simplified wing-flap configuration. The configuration consist of an extended NACA0012 aerofoil as the wing, along with a NACA0012 aerofoil as the flap, which was previously used in the VALIANT project. The Computational Fluid Dynamic (CFD) simulations and Computational Aeroacoustic (CAA) simulations were conducted using IDDES and FW-H methods. Effects of DBD plasma actuator is modeled based on S-H model.

II. Numerical Models

The three-dimensional wall resolved turbulent flow around the wing-flap configuration is simulated using the compressible SST k-ω base IDDES [14] method using the commercial solver STARCCM+. The IDDES method, based on a blending factor, uses the second order upwind for the RANS regions and central differencing scheme for the LES region. A converged steady state k-ω SST solution has been used as the initial solution for the IDDES. Far-field noise is calculated using Farassat's 1A Formulation [15], which is a non-convective form of the Ffowcs Williams-Hawkings (FW-H) Formulation [16]. A permeable integral surface is used to collect the source data for the FW-H. The acoustic suppression zone model [17] has been used to damp pressure waves and minimize spurious reflections from the free stream boundary.

Effect of the plasma actuator is modeled based on the Suzen and Huang model [12], where the body force field, due to plasma, is calculated using the electric field (E) and charge density field (ρ_c).

$$\vec{f_b} = \rho_c \vec{E}. \tag{1}$$

A Gaussian function has been used to model the charge density on the wall.

$$\rho_{c(wall)} = \rho_c^{max} G(x), \tag{2}$$

where the Gaussian function is,

$$G(x) = exp\left[\frac{-x^2}{2\sigma^2}\right]. \tag{3}$$

Here, x is 1D coordinate relative to the reference point x = 0, which is the surface closest to embedded electrode and exposed electrode. $\sigma/L = 0.3$ where σ being the width of embedded electrode. The calculated body-force field is then added to the momentum equations as a source term. The body-force field due to plasma is assumed to be constant in time, hence the effects due to the AC frequency is ignored.

III. Methodology

A. CFD Domain and Boundary Conditions

The geometric configuration of CFD/CAA analysis is based on the experimental setup defined in the (Innovative Methodologies and technologies for reducing Aircraft noise Generation and Emission) IMAGE project, where a NACA0012 profiles have been used to represent the wing and the flap.The wing is an extended NACA0012 aerofoil using a flat plate with a 15 mm maximum thickness and a 0.6 m chord. The flap is a NACA0012 aerofoil with a 0.1 m chord. The leading edge of the flap is located (-20 mm, -15 mm) relative to the trailing edge of the wing. The flap is deflected 5°, relative to an axis located at its leading edge. The wing and flap trailing edge thickness are 0.32 mm and 0.25 mm respectively. Figure 1 shows the computational domain. It is a cylindrical domain with an acoustic suppression zone that is used to minimize acoustic reflections from the free stream boundary. The acoustic suppression zone has a thickness equal to the chord of the flap. The free-stream boundary is located in the circumference of the cylinder. The Mach number at the free stream boundary is set to 0.147 (Speed of sound is 340 m/s) in order to mimic the free stream velocity used in the VALIANT project; 50 m/s. The Reynolds number relative to the chord of the wing is 2×10^6 and relative to the chord of the flap 3.3×10^5. The span of the domain is 30% of C_{flap}, yielding a 1.3% blockage. A permeable surface, that has no influence to the CFD simulation, has been placed $2C_{flap}$ from the wing, in order to accumulate source data for the FW-H. The turbulence intensity at the free stream boundary is set to be 1%. Side boundaries are defined as periodic. The wing and flap surfaces are defined as no-slip walls.
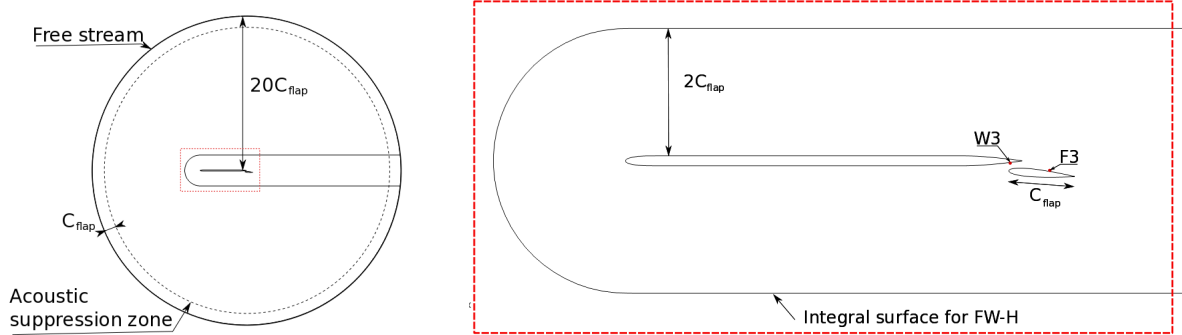

Fig. 1   LHS: The computational domain and the boundary conditions. RHS: Zoom of the wing-flap configuration. W3 and F3 are pressure probes. W3 located at 10 mm upwind from the trailing edge of the wing. F3 located at 45 mm from the trailing edge of the flap. F3 is also the location of the plasma actuator.

Two point probes are used to analyze the unsteady pressure (W3 and F3) on the wing and the flap [18]. The W3 probe is located 10 mm from the trailing edge of the wing, and the F3 probe is located at 45 mm from the trailing edge of the flap. Figure 2 shows a zoom of the tetrahedral computational mesh with prism layers. Approximately 270 nodes/C_{flap} are used close to walls [19]. The span-wise and chord-wise cell size is constant. The grid points near the wall have a y^+ value below unity. The trailing edge region of both the wing and flap are refined in order to capture the detailed effects of vortex shedding.

A converged steady state k-ω SST solution was used to initialize the unsteady IDDES simulation which ran with a $\Delta t = 1 \times 10^{-5}$ s for 0.12 s. Each time step used 10 inner iteration. Time averaging of aerodynamic data and sampling of acoustic data has been started when the simulation reached a statistically steady state at 0.05 s.
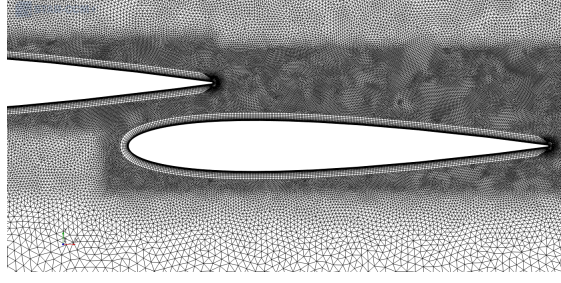
Fig. 2   The tetrahedral computational mesh with prism layers closer to walls.

B. Validation of the CFD model

The simulation with a flap deflection angle of 0° was used for the validation of the CFD simulation. Here, the aerodynamic data such as mean velocity and mean pressure have been compared with the VALIANT experimental data. The converged IDDES solution, Figure 3, shows the boundary layer profiles at -300 mm, -200 mm and -100 mm, that reasonably agree with the experimental data. Numerical results closer to the trailing edge of the wing (-100 mm) indicate the largest difference. This is due to the use of no slip boundary conditions, where the actual roughness of the experimental aerofoil is ignored.
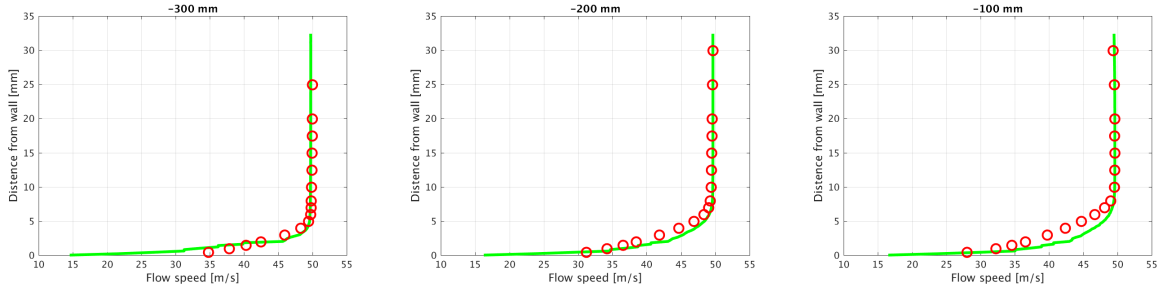

Fig. 3   Boundary layer profiles of the pressure side of the wing at -300 mm, -200 mm and -100 mm from the trailing edge, compared with the VALIANT experimental data (◯) [18]. x = 0 is the trailing edge of the wing. The flap deflection angle is 0° **and the free stream velocity is 50 m/s.**

Figure 4 compares the pressure side C_p with the experimental data. In the wing-flap configuration with a 0° flap deflection angle, the pressure side is located on the bottom surface of the wing, and the top surface on the flap. Results show a good agreement with the experimental data. At about -0.8 x/c_{flap}, on the bottom surface of the wing, a slight bump in pressure is visible and this is due to flow transition. On the top surface of the flap, the flow transition is at about 40% of C_{flap}.
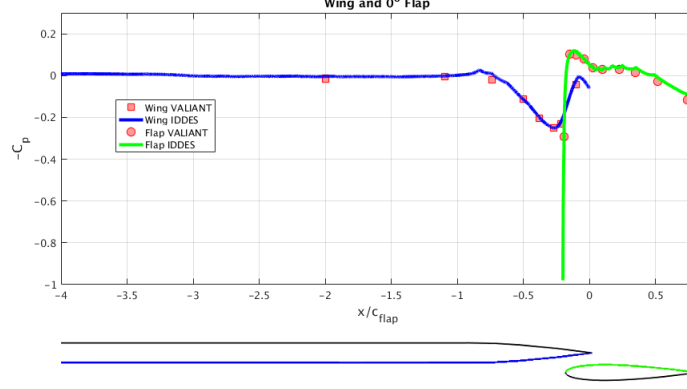
Fig. 4 **Pressure coefficient at the mid-span bottom surface of the wing (—) and mid-span top surface of the flap (—) compared with the VALIANT experimental data [18]. The flap deflection angle is $0°$ and the free stream velocity is 50 m/s.**

Figure 5 shows surface pressure spectra at the locations W3 and F3, compared with the VALIANT experimental data. Pressure spectra show a reasonable agreement with the VALIANT experiments. Frequencies below 150 Hz differ from the experimental data due to the IDDES simulation limited run time. The pressure spectrum at the F3 probe diverges from the experimental data at frequencies above 6 kHz. This indicates unresolved near-wall small scale eddies of the IDDES. These surface pressure probes also give evidence about dipole acoustic sources [19].
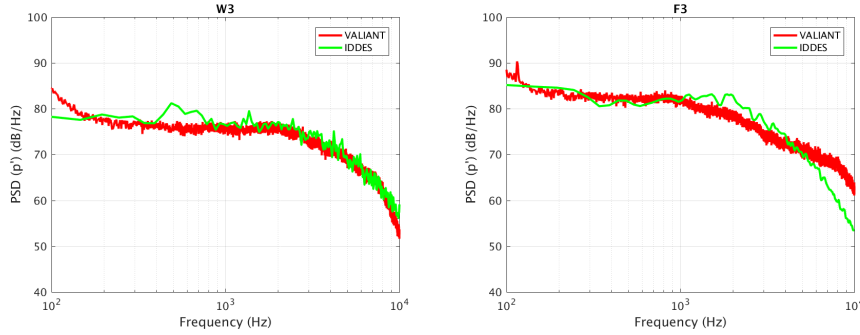

Fig. 5 **Surface pressure spectra at the locations W3 and F3, compared with the VALIANT experimental data. The flap deflection angle is $0°$ and the free stream velocity is 50 m/s.**

C. DBD plasma domain and boundary conditions

A two dimensional domain of a flat plate has been used for calculating the body force field due to the effects of a DBD plasma actuator. Initially, the electric field was resolved based on the given electric potentials; 5 kV and 20 kV. Then the charge density field was resolved separately using the modeled wall charge density for each of these cases. The Gaussian function, that was used for modeling the charge density of the wall, has been calibrated using the maximum charge density field values given in the work by Brauner et al.[20]. For the case where voltage is 5 kV, the charge density is $\rho_c^{(max)} = 7.5 \times 10^{-3} C/m^3$ and for the case of 20 kV, $\rho_c^{(max)} = 2 \times 10^{-3} C/m^3$.

D. Validation of the DBD plasma model

The DBD plasma model was validated using the experimental data by Benard et al. [21]. Here, the body force field was added as a source term to the momentum equation of the CFD simulation with no external flow. As a result, the converged velocity field appeared as a jet that blows the flow towards the direction of the encapsulated electrode.

Figure 6 shows that the simulation closely match with the experimental data. However, experimental flow looks slightly stronger compared to the results of the numerical model.
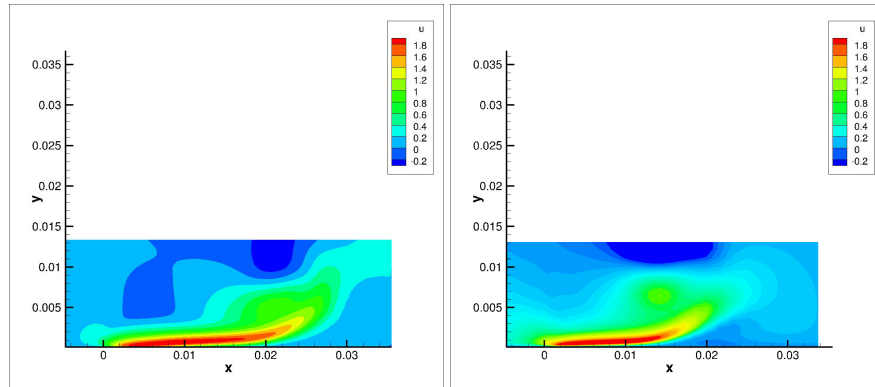

Fig. 6   Left: the experimental [21] U velocity measured using PIV. Right: simulation results using the Suzen and Huang model on a 2D flat plate.

IV. Results

A baseline case with a 5° flap deflection angle has been simulated on the same domain with the same mesh configuration as in the validated 0° test case. In order to evaluate the effects of plasma, two other simulations were conducted by applying body forces corresponding to 5 kV and 20 kV electric potentials. The plasma actuator was placed on the top side of the flap at 45 mm from the trailing edge. This point is located upstream of the point to flow separation. Figure 7 shows the body force contours of the plasma at 5 kV potential. Highest magnitude of body force is shown at a location on the surface of the aerofoil, which has minimum distance to the exposed and encapsulated electrodes. The strength of plasma forces gradually decays towards the direction of the encapsulated electrode.
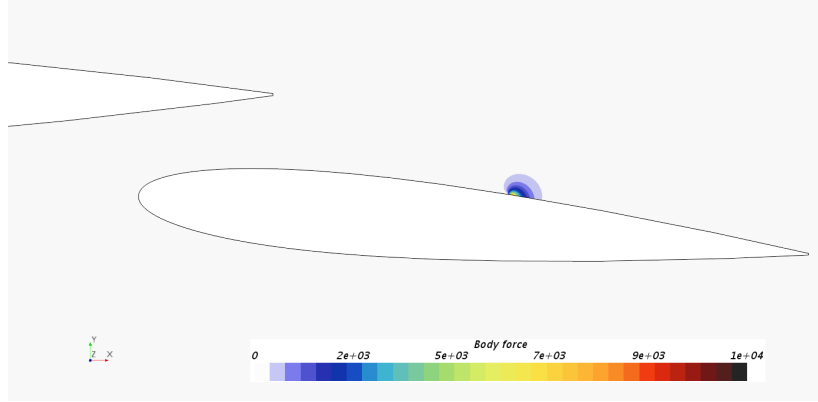

Fig. 7   Body force magnitude of plasma, f_b.

A. Aerodynamic Result

Figure 8 shows the C_p and C_{Prms} on the mid-span surface of the flap. The predicted C_p profile does not show any significant change due to plasma, however, C_{Prms} shows reduced values, towards downstream direction, from the point where plasma forces are implemented. This indicates a reduction of the surface pressure fluctuations from 60% to 90% of the chord of the flap, therefore a possible reduction of the acoustic dipole sources that originate from the flap. Figure 9 shows the iso-surfaces of instantaneous vorticity at 7000 s^{-1}, without plasma forces. The figure illustrates vortex structures, that originated from the trailing edge of the wing, and their interact with the trailing edge of the flap.
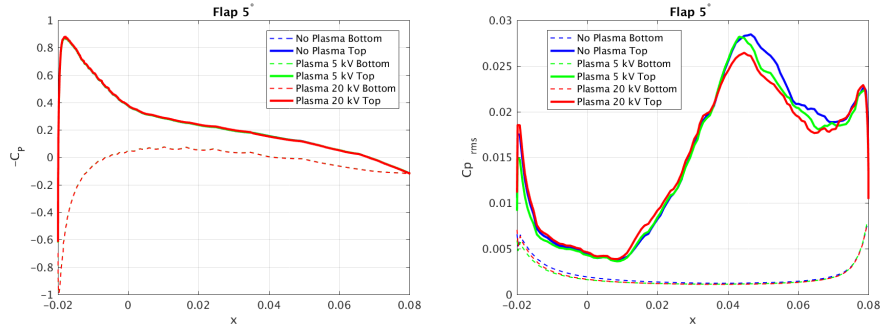

Fig. 8   Predicted pressure coefficient C_p and C_{Prms} on flap surface at the mid span. The plasma actuator is located on the top surface at 55% of C_{flap}.

B. Aeroacoustic Result

Figure 10 shows the frequency spectra at a receiver located $3C_{wing}$ below the mid-chord of the wing. Up to 2.5 dB noise reduction is evident at frequencies below 1 kHz. There is no recognizable noise reduction at high frequencies. Noise reduction increases with respect to the electric potential. The maximum noise reduction is observed towards at 210° to 330°, which covers the possible urban regions closer to airports during take off and landing.
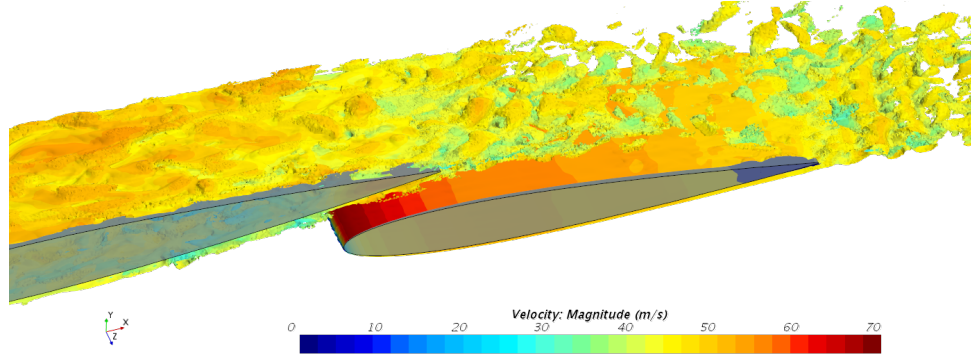
7

Fig. 9   Iso-surface of vorticity of 7000 s^{-1} of the case with 20 kV plasma, coloured by the velocity.
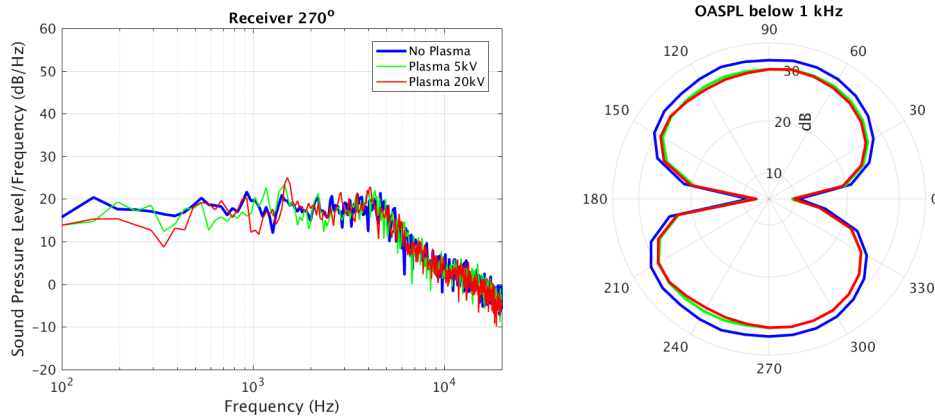

Fig. 10   left: Acoustic spectrum of a receiver located at $3C_{wing}$ below the centre of the wing-chord. right: OASPL at frequencies below 1 kHz

V. Conclusion

IDDES simulations of two wing-flap configurations (flap deflection angle 0°, 5°) were performed to estimate the far field noise due to turbulent aerodynamic flow. The simulation of flap deflection angle 0° was used to validate the results. The simulation of flap deflection angle 5° was then used with the DBD plasma model. The presence of DBD actuator has energized, as desired, the boundary layer with a somewhat slightly increased favorite pressure gradient in the stream-wise direction. Aerodynamic results also indicate relatively low C_{Prms} downstream of the plasma actuator, which consequently reduced the far field low frequency noise (below 1 kHz) by maximum 2.5 dB. The noise reduction is larger when the body force, produced by plasma, is increased. The noise reduction, due to DBD plasma actuators, are more evident towards the directions perpendicular to the chord of the wing, which includes the possible urban areas near airports that are affected by the airframe noise.

References

[1] LeVine, M. J., Bernardo, J. E., Zanella, P., Kirby, M., and Mavris, D. N., "Placement of Runways at Capacity Constrained Airports to Minimize Population Exposure to Noise," *2018 Aviation Technology, Integration, and Operations Conference*, 2018, p. 3995.

[2] AIRBUS, *Getting to Grips with Aircraft Noise.*, 2003.

[3] Gly, D., and Delfs, J., "Aeroacoustic installation effects on transport aircraft research at Onera and DLR," *16th Workshop of the Aeroacoustics Specialist Committee of CEAS and 2nd Workshop of the European X-Noise EV network, Braunschweig*, 2012.

[4] Lockard, D. P., and Lilley, G. M., "The airframe noise reduction challenge," *NASA/TM–2004–213013*, 2004.

[5] Leylekian, L., Lebrun, M., and Lempereur, P., "An overview of aircraft noise reduction technologies." *AerospaceLab*, , No. 6, 2014, p. 1.

[6] Salas, P., and Moreau, S., "Aeroacoustic simulations of a simplified high-lift device accounting for some installation effects," *AIAA Journal*, Vol. 55, No. 3, 2016, pp. 774–789.

[7] Li, Y., Wang, X., and Zhang, D., "Control strategies for aircraft airframe noise reduction," *Chinese Journal of Aeronautics*, Vol. 26, No. 2, 2013, pp. 249–260.

[8] Wang, J.-J., Choi, K.-S., Feng, L.-H., Jukes, T. N., and Whalley, R. D., "Recent developments in DBD plasma flow control," *Progress in Aerospace Sciences*, Vol. 62, 2013, pp. 52–78.

[9] He, C., Corke, T. C., and Patel, M. P., "Plasma flaps and slats: an application of weakly ionized plasma actuators," *Journal of Aircraft*, Vol. 46, No. 3, 2009, pp. 864–873.

[10] Post, M. L., and Corke, T. C., "Separation control on high angle of attack airfoil using plasma actuators," *AIAA journal*, Vol. 42, No. 11, 2004, pp. 2177–2184.

[11] Peng, S.-H., "Shear-layer manipulation of backward-facing step flow with forcing: A numerical study," *10th Symposium of ECORFTAC Experimental Turbulent Modelling and Measurements*, 2014.

[12] Suzen, Y., Huang, G., Jacob, J., and Ashpis, D., "Numerical simulations of plasma based flow control applications," *35th AIAA Fluid Dynamics Conference and Exhibit*, 2005, p. 4633.

[13] Orlov, D., Corke, T., and Patel, M., "Electric circuit model for aerodynamic plasma actuator," *44th AIAA Aerospace Sciences Meeting and Exhibit*, 2006, p. 1206.

[14] Shur, M. L., Spalart, P. R., Strelets, M. K., and Travin, A. K., "A hybrid RANS-LES approach with delayed-DES and wall-modelled LES capabilities," *International Journal of Heat and Fluid Flow*, Vol. 29, No. 6, 2008, pp. 1638–1649.

[15] Farassat, F., "Derivation of Formulations 1 and 1A of Farassat," *NASA/TM-2007-214853*, 2007.

[16] Williams, J. F., and Hawkings, D. L., "Sound generation by turbulence and surfaces in arbitrary motion," *Phil. Trans. R. Soc. Lond. A*, Vol. 264, No. 1151, 1969, pp. 321–342.

[17] Kim, J. W., H. Lau, A. S., and Sandham, N. D., "Proposed boundary conditions for gust-airfoil interaction noise," *AIAA journal*, Vol. 48, No. 11, 2010, pp. 2705–2710.

[18] Lemoine, B., "Etude aéroacoustique de configurations génériques de dispositifs hypersustentateurs: approches analytique et expérimentale," Ph.D. thesis, Ecully, Ecole centrale de Lyon, 2013.

[19] Wasala, S. H., Storey, R. C., Norris, S. E., and Cater, J. E., "Aeroacoustic noise prediction for wind turbines using Large Eddy Simulation," *Journal of Wind Engineering and Industrial Aerodynamics*, Vol. 145, 2015, pp. 17–29.

[20] Brauner, T., Laizet, S., Benard, N., and Moreau, E., "Modelling of dielectric barrier discharge plasma actuators for direct numerical simulations," *8th AIAA Flow Control Conference*, 2016, p. 3774.

[21] Benard, N., Caron, M., and Moreau, E., "Evaluation of the time-resolved EHD force produced by a plasma actuator by particle image velocimetry-a parametric study," *Journal of Physics: Conference Series*, Vol. 646, IOP Publishing, 2015, p. 012055.